RSC Advances

PAPER

View Article Online
View Journal | View Issue

Cite this: *RSC Adv.*, 2025, **15**, 13225

Adsorption/photodegradation of methylene blue using a sulfur-1,3-diisopropenylbenzene copolymer†

Moyan Wu,[a] Yue Liu,[a] Lili Wu,[a] Tom Hasell *[b] and Fang Luan *[ab]

This study aims to utilize sulfur-1,3-diisopropenylbenzene (S-DIB) to develop a more cost-effective treatment method for dye-contaminated wastewater. The behavior and mechanisms of adsorption and photodegradation on the removal of methylene blue (MB) by S-DIB in water were studied systematically, including three isotherm model fitting tests, kinetics and thermodynamic analysis. With the optimization of the adsorption experimental conditions, the results revealed that S-DIB achieved a 96.53% removal percentage of MB at pH 11, initial dye concentration of 8 mg L^{-1}, adsorbent dose of 20 mg, temperature of 293 K and contact time of 180 min. The adsorption data fitted well with the Langmuir isotherm and pseudo-second order models, with regression coefficients (R^2) of 0.9990 and 0.9993, respectively. Thermodynamic studies showed that the adsorption of MB by S-DIB was exothermic and spontaneous. Furthermore, S-DIB exhibited a unique photodegradation property in visible light regions with the removal of MB from water, offering a dual mechanism of adsorption and photodegradation, with a degradation efficiency is 94%. This work enhances the possibilities and potential for the application of sulfur-rich copolymers in wastewater treatments.

Received 22nd February 2025
Accepted 12th April 2025

DOI: 10.1039/d5ra01297j

rsc.li/rsc-advances

Introduction

Water is a vital resource for sustaining life on Earth, and access to clean water is essential for maintaining both human health and the stability of the ecosystems. Nevertheless, during the last decades, the extensive presence of organic dye in wastewater from textile and paper manufacturing industries has caused considerable environmental pollution. The substantial amount of harmful substances and carcinogenic compounds in dye effluents can cause hazards to the human health, even at extremely low concentrations. Therefore, the removal of organic dyes from wastewater is imperative.[1,2]

At present, the adsorbents commonly used in methylene blue adsorption are composite membrane materials,[3] biomass materials,[4–6] and chemically modified carbon materials.[7,8] About 70 million tons of elemental sulfur, which is generated as a by-product of hydrogenation desulfurization, is stored in open areas in petrochemical industries each year,[9] potentially threatening the environment (such as soil, water and creatures) when it flows with wind or rain. Therefore, effectively utilizing large quantities of by-products to solve dye pollution in waste water is mutually beneficial.[10–12] In 2013, Pyun and his group pioneered a groundbreaking method known as "inverse vulcanization," which facilitated the extensive copolymerization of liquid elemental sulfur and vinylic comonomers. This innovative approach eliminated the requirement for external initiators or organic solvents, making the reaction simple and economical; accordingly, sulfur-1,3-diisopropenylbenzene (S-DIB) was first synthesized as an inverse vulcanization product.[13] The miscible sulfur diisopropenylbenzene copolymer (S-DIB) is a shape persistent stable polymer; its current applications are in batteries to enhance battery performance[14–16] and as stretching materials.[17,18] Similar inverse vulcanization reaction products have been widely studied and applied in various fields, such as infrared imaging,[19] cathodes of Li–S batteries, sorbents for oil spills, metal and organic decontamination,[20,21] and matrices for slow-release fertilizers and antimicrobial materials.[22]

Sulfur-rich polymers for adsorption and photodegradation have been reported, including elemental sulfur polymers with sunflower oil to absorb heavy metal ions,[23] gasoline and diesel in water.[24,25] A novel series of high sulfur polymers containing fatty acids, such as oleic acid (OA), linoleic acid (LA) and linolenic acid (LnA), were synthesized *via* inverse vulcanization, which offered superior sensitivity for the removal of MB dye from aqueous solutions, cooperating with magnetic and TiO_2 nanoparticles in composites, and the photodegradation activity of the sulfur co-polymers was improved significantly.[26] The formation of porous sulfur polymers (PSPs) *via* template fabrication of pores with table salt during the synthesis of S-DIB

[a]*Department of Chemistry and Chemical Engineering, School of Pharmacy, Jiamusi University, Jiamusi 154007, Heilongjiang, China. E-mail: fangl_chem@126.com*
[b]*Department of Chemistry, University of Liverpool, Liverpool L69 7ZD, UK. E-mail: t.hasell@liverpool.ac.uk*

† Electronic supplementary information (ESI) available: FT-IR, TGA spectra, *etc.* See DOI: https://doi.org/10.1039/d5ra01297j

could intensively adsorb and chemically neutralize organic contaminants such as caffeine.[27] Nevertheless, research on the application of S-DIB as an adsorbent for the removal of organic dye pollutants has not yet been reported. Consequently, we utilized a simply synthesized and low-cost copolymer sulfur-1,3-diisopropenylbenzene as an adsorbent and explored its influencing factors and adsorption mechanism, including the adsorption isotherm and adsorption thermodynamics for methylene blue. This study aims to enrich the application fields of sulfur copolymers and provide references for wastewater treatment.

Methods

Reagents and materials

All the chemicals are commercially available and used without further purification. Elemental sulfur (S_8, sublimed powder, reagent grade, $\geq$ 99.5%) was purchased from Harbin Reagent Chemical Plant. 1,3-diisopropenylbenzene (stabilized with TBC, >97%) and methylene blue (MB) were purchased from Macklin.

Preparation of S-DIB

Polymerization of inverse vulcanization was carried out in an open glass vial of 30 mL volume on aluminum heating blocks. The vial was heated to 159 °C, and 3 g elemental sulfur was added. The sulfur completely melted in few minutes from light yellow powder to yellow-orange liquid under continuous stirring. Subsequently, 3 g DIB was introduced dropwise into the molten sulfur, and the mixture was stirred at 185 °C for 8–10 min until the reaction was completed. Finally, the product was cooled to room temperature (Fig. 1).[13] According to this method, S-DIB samples with a mass ratio of elemental sulfur to DIB monomer ranging from an equal 50 : 50 split to a significantly higher 95 : 5 proportion were prepared.

Characterization of S-DIB

The structural and compositional analyses of the S-DIB were carried out using a combination of advanced analytical methods. Scanning electron microscopy (SEM) imaging coupled with energy-dispersive X-ray spectroscopy (EDS) was conducted on an FEI Inspect F system, operating at an acceleration voltage ranging from 10 to 20 kV. To ensure optimal electrical conductivity with SEM imaging, the samples were coated with a fine layer of gold using an automated sputter coater. Fourier-transform infrared (FTIR) spectroscopy was performed using a NEXUS-670 instrument, capturing spectra across a wavenumber ranging from 500 cm^{-1} to 4000 cm^{-1}. For Nuclear Magnetic Resonance (NMR) analysis, a Bruker NEO spectrometer operating at 400 MHz was employed, with deuterated chloroform serving as the solvent and tetramethylsilane (TMS) as the internal reference.

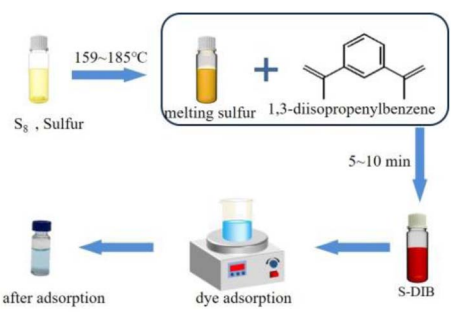

Fig. 1 Synthesis scheme and adsorption/photodegradation application of S-DIB for MB removal.

Adsorption experiments of MB

S-DIB was added to the MB aqueous solution and then agitated on a hot plate at 300 rpm using a 25 mm × 7 mm magnetic stirrer bar. At various times, 3 mL samples were withdrawn and passed through a 0.22 μm filter to measure the remaining concentrations of MB at 664 nm (ref. 28) using an ultraviolet spectrophotometer (UV-2550, Shimadzu, Japan).

The experiments used a batch approach to investigate the effects of various factors, including pH, adsorbent amount, duration of contact, initial concentration, and temperature. The role of pH was analyzed using 0.1 mol L^{-1} NaOH or 0.1 mol L^{-1} HCl to adjust the pH in the range of 3–11. The effect of adsorbent dosage was explored by adjusting quantities ranging from 5 mg to 120 mg. The effects of contact time ranging from 30 to 180 minutes, temperature ranging from 293 K to 318 K, and initial concentration of MB ranging from 2 to 16 mg L^{-1} were assessed.

Based on the remaining concentrations of MB, the efficiency of removal and the capacity for adsorption were calculated using eqn (1) and (2), respectively.[29]

$$R(\%) = \frac{c_0 - c_e}{c_0} \quad (1)$$

$$q_e = (c_0 - c_e) \times \frac{V}{m} \quad (2)$$

where R (%) is the removal efficiency, c_0 (mg L^{-1}) is the initial MB concentration, c_e (mg L^{-1}) is the equilibrium concentration of MB, q_e (mg g^{-1}) is the equilibrium adsorption capacity of the adsorbent for MB, m (g) is the dry weight of the material and V (L) is the solution volume.

Results and discussion

Preparation results of the S-DIB

A series of transparent red glassy copolymer S-DIB were obtained *via* inverse vulcanization. This indicates that the viscosity progressively increased with higher DIB content for samples that contained 5–25 wt% DIB. However, the 50 wt% DIB sample demonstrated a sharp reduction in the viscosity, which is beneficial for adsorption generation.

Characterization results of S-DIB

Fig. 2 displays the ^{1}H NMR spectra of S-DIB (50%) in a solvent of $CDCl_3$, in which the signal peaks indicate the formation of S-DIB by sulfur and DIB through copolymerization. It was found that the alkene proton signal at δ = 5.00–5.40 ppm of DIB

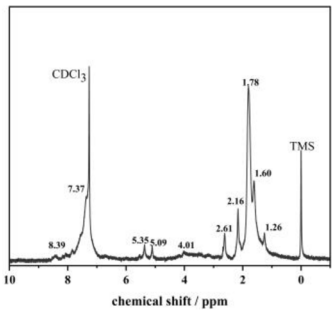

Fig. 2 ^{1}H NMR spectra of the S-DIB (50%) copolymer in $CDCl_3$.

became extremely weak, which confirmed that DIB almost reacted with sulfur completely during the crosslinking process. Furthermore, the ^{1}H NMR spectra confirmed the existence of aromatic proton signals at δ = 7.37–8.39 ppm and methyl proton signals at δ = 1.26–2.16 ppm.

As shown in Fig. S1,† the FTIR spectra of DIB and S-DIB with various mass ratios were determined. The strong absorption band at 1630 cm^{-1} is attributed to the stretching vibration of exocyclic C=C groups in DIB, while the peaks of several S-DIB with different mass ratios at the same wavenumber vanish. In addition, compared to the stretching vibration peak of the exocyclic = C–H groups at 3080 cm^{-1} in DIB, these peaks in S-DIB became very weak. The peak at 887 cm^{-1} is attributed to the out-of-plane bending vibration of the = C–H alkene groups in DIB, and the signals of S-DIB disappeared after crosslinking. These facts confirmed the occurrence of polymerization between DIB and sulfur. The characteristic peaks of C–S bonds can be observed at 1120 cm^{-1} and 695 cm^{-1} in the FTIR spectra of S-DIB, confirming that the π bonds of C=C groups in DIB are broken up and the alkene carbon is combined with sulfur.[30] This further confirmed the successful synthesis of S-DIB.

The thermal stability evaluation of S-DIB by TGA is shown in Fig. S2,† which illustrates that the decomposition temperature of S-DIB is 207.82 °C. Within the temperature range of 199–296 °C, the mass loss of S-DIB significantly increases. The mass change during this stage is mainly attributed to the breaking of S–S bonds inside S-DIB molecules and the cross-linking and degradation reactions of the copolymer chains. These chemical changes lead to the reorganization of the copolymer structure and a decrease in mass. Compared with pure sulfur, the decomposition temperature of the S-DIB copolymer is higher, which proves that cross-linking between organic molecules and S_8 enhances the network structure of the polymer.[23] Therefore, S-DIB material has significant advantages in thermal stability because it can withstand higher temperatures without rapid decomposition, thus exhibiting better performance in high-temperature environments. As the temperature continued to increase from 296 °C to 600 °C, the mass fraction of the material changed from 35.5% to 25.5%, which indicated that more stable inorganic sulfides and highly cross-linked carbon skeletons may remain after the polymer material collapses.[31]

SEM images (Fig. 3a and b) showed the changes in the S-DIB surface before and after adsorption. Being a kind of glassy

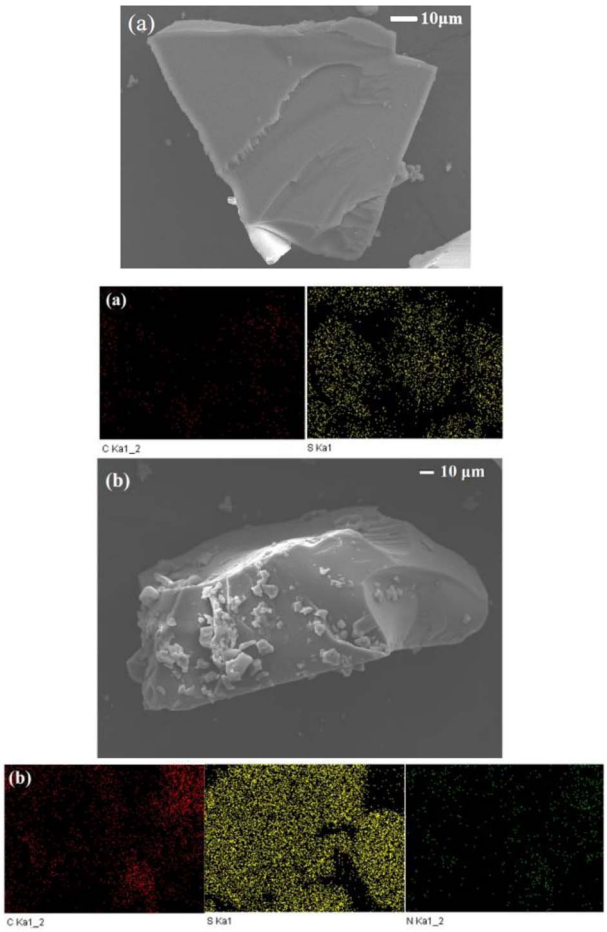

Fig. 3 SEM images of 50% S-DIB (a) before adsorption (inset: EDS of S-DIB before adsorption) and (b) after adsorption (inset: EDS of S-DIB after adsorption).

copolymer, the surface of the S-DIB product is notably smooth without any adhesion before the adsorption experiments. Compared with the spectra before adsorption, the EDS spectra after adsorption not only retained the original S and C elements but also presented abundant N element signals. In fact, there are only three substances in the adsorption experimental system: S-DIB, MB and water. As a result, the N element signal observed in EDS can come from only the MB molecule. Consequently, the appearance of the N element signal is important evidence of the successful adsorption of methylene blue on the S-DIB surface.[32]

Effects of MB adsorption

Effect of sulfur content. Polymers with varying sulfur concentrations were synthesized to investigate the impact of sulfur content on MB adsorption efficiency. The data revealed a distinct pattern (Fig. 4). As sulfur mass ratios increased within the range of 50–100%, the adsorption capacity (q_e) took a noticeable dip; the q_e values of S-DIB are 7.72, 6.14, 2.46, 1.53, and 0.15 mg g^{-1}. The adsorption capacity of polymer S-DIB reached its maximum (7.72 mg g^{-1}) at a sulfur content of 50 wt%. Thus, 50 wt% S-DIB polymers were selected for further study.

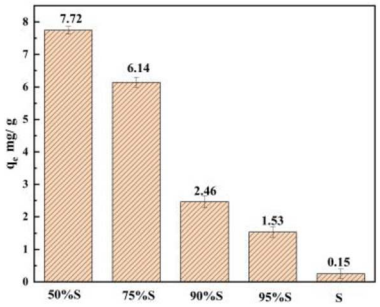

Fig. 4 Adsorption capacity of S-DIB with different sulfur mass ratios (50–100% sulfur, $c_0 = 8$ mg L^{-1}; $m = 20$ mg; $T = 293$ K; $t = 180$ min; and pH = 11.0).

Effect of adsorbent dose. Fig. S3† illustrates the effects of the S-DIB dosage on MB adsorption efficiency. The adsorption efficiencies of S-DIB at masses of 5, 10, 15, 20, 30, and 50 mg in 20 mL 8 mg L^{-1} MB aqueous at 293 K and pH = 11.0 were 47.2%, 72.83%, 86.68%, 96.65%, 96.7%, and 96.82%, respectively. When the dose of S-DIB increased from 5 mg to 20 mg, the adsorption efficiency of MB increased from 19.9% to 96.65%. A possible reason is that the active sites of S-DIB increase with an increase in adsorbent content.[33] In addition, it can be noted that when the dosage of S-DIB increased from 20 mg to 50 mg, its adsorption efficiency for MB changed from 96.65% to 96.82%, with only a 0.17% change in adsorption efficiency. The reason may be due to the limited active sites on the surface of S-DIB. At a certain concentration of MB solution, when the adsorbent content increases to a certain extent, the adsorbate molecules already occupy most of the available active sites.[34]

Therefore, considering the cost-effectiveness and adsorption performance, 20 mg of S-DIB adsorbent was selected for subsequent MB adsorption experiments.

Effect of pH. The pH level of the medium stands out as a critical factor in the adsorption process, wielding significant influence over both the surface charge of the adsorbent and the structural characteristics of the chemical compound involved. This variable can dramatically shape the efficiency and dynamics of adsorption, making it a key player in determining overall outcomes. Therefore, the effect of pH on MB adsorption was investigated.

Fig. S4† shows that with an increase in pH from 3 to 11, the adsorption efficiency of S-DIB on MB increased. To determine the surface charge of S-DIB, the zeta potential of the material was tested at pH = 3–11. The result is shown in Fig. S5; † pH_{zpc} of 50 wt% S-DIB was 3.47. If pH > pH_{zpc}, the zeta potential gradually decreases, and the adsorbent S-DIB carries a negative charge, which makes it easy to adsorb cationic dyes, such as MB, due to the electrostatic attraction between the adsorbent and the dye. As the pH value continued to increase, the zeta potential of S-DIB with different sulfur contents gradually decreased, and its overall trend echoed the trend of MB adsorption. In other words, the adsorption capacity of S-DIB was significantly enhanced under alkaline conditions, and the ideal pH level for this adsorption was found to be 11.0.

Effect of initial MB concentration. Fig. S6† shows the effect of the initial MB concentration on the adsorption capacity and efficiency of S-DIB. The loading capacity of S-DIB on MB increased with the enhancement of MB concentration in the range of 2–16 mg L^{-1}. The adsorption almost reached an equilibrium at an MB concentration of 8 mg L^{-1}, which is attributed to the saturation of the adsorption site of S-DIB. Its adsorption ratio reached 96.65%, and the saturated adsorption amount of S-DIB was 7.72 mg g^{-1}. Therefore, the optimum initial concentration of MB was determined to be 8 mg L^{-1}.

Effect of contact time. Fig. S7† shows the effect of the adsorption time of MB. Apparently, S-DIB adsorbed MB rapidly and reached adsorption equilibrium within 180 min. During the first few minutes, the S-DIB surface exhibited enough adsorption sites to capture MB. Later, as MB gradually filled, the S-DIB surface largely occupied the adsorption sites, and the adsorption capacity was approximately constant. Thus, the adsorption material has reached the saturation capacity.[35] The ideal adsorption duration was determined to be 180 minutes. The adsorption process can be characterized by three distinct phases: the initial rapid adsorption taking place during the first 50 minutes, a slower phase from 50 to 180 minutes, and the equilibrium phase beyond 180 minutes. In the initial phase, dye molecules quickly spread across the adsorbent's surface due to mass transfer. As many active functional groups on the adsorbent become occupied by the dye, the subsequent diffusion of dye molecules from the surrounding layer into the adsorbent's surface and inner regions occurs at a much slower rate, eventually leading to a dynamic equilibrium in adsorption.[36] Consequently, the optimal time for the adsorption of MB by S-DIB was established at 180 minutes.

Effect of temperature. Temperature (T) impacted the adsorption efficiency of the adsorbent. Thus, the MB adsorption of S-DIB was investigated in the temperature range of 293–318 K. As the temperature increased, the adsorption rate of MB decreased from 96.53% to 64.71% (Fig. S8†), indicating that the adsorption process is exothermic.[37] Consequently, lower temperatures are beneficial for the adsorption of MB.

Based on the previous experiments, the optimal adsorption conditions were determined as follows: 20 mg of S-DIB dosage, pH of 11.0, temperature of 293 K, and contact time of 180 min. Under the optimized experimental conditions above, the adsorption capacity of the S-DIB copolymer on MB was 7.72 mg g^{-1}, and the adsorption efficiency was 96.53%.

Adsorption isotherms. The isothermal data of MB were characterized using the Langmuir model and the Freundlich model at 293 K to further uncover the adsorption mechanism of MB by S-DIB. The linear equations of these two models are presented as eqn (3) and (4), respectively.[38] The fitting curves are depicted in Fig. 5(a) and (b). The fitting parameters of the models are tabulated in Table 1.

$$\frac{c_e}{q_e} = \frac{1}{q_m K_L} + \frac{c_e}{q_m} \quad (3)$$

$$\ln q_e = \ln K_f + \frac{1}{n} \ln c_e \quad (4)$$

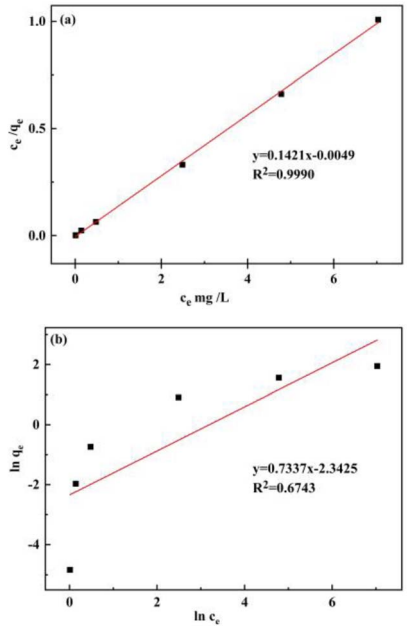

Fig. 5 Fitting curve of the (a) Langmuir model and (b) Freundlich model.

Table 1 Fitting parameters of isotherm models

Langmuir model			Freundlich model		
q_m (mg g^{-1})	K_L (L mg^{-1})	R^2	n	K_f	R^2
7.22	0.184	0.9990	3.95	2.24	0.6743

where q_m (mg g^{-1}) is the monolayer saturation adsorption capacity, K_L (L mg^{-1}) is the adsorption equilibrium constant, and K_f and n are the Freundlich constants. c_e is the concentration of the solution when adsorption equilibrium is achieved.

The correlation coefficient (R^2) of the Langmuir model (0.999) is greater than that of the Freundlich model (0.6743), which indicates that the adsorption isotherms are consistent with the Langmuir model and are in accordance with monolayer adsorption behavior. In this adsorption condition, the sites on the adsorbent's surface are uniformly spaced, allowing each site to accommodate just one molecule of the adsorbate, with no interactions occurring between the adsorbate molecules.[39]

For the sake of an in-depth discussion of the interaction between S-DIB and MB, we fitted a Dubinin–Radushkevich (D–R) model that estimates the mean adsorption energy (E), which may be used to predict the mechanisms involved in adsorption (eqn (5) and (6)). Physical adsorption, ion exchange and chemical adsorption corresponding to the values of E are less than 8 kJ mol^{-1}, 8–16 kJ mol^{-1} and greater than 16 kJ mol^{-1}, respectively.[40]

$$\varepsilon = RT \ln\left(1 + \frac{1}{C}\right) \quad (5)$$

$$E = \frac{1}{\sqrt{2\beta}} \quad (6)$$

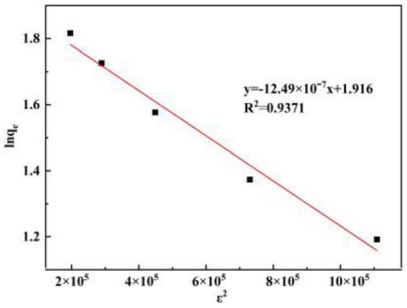

Fig. 6 Fitting curve of the Dubinin–Radushkevich model.

where E is the energy of adsorption, as described in the D–R isotherm model; β represents the activity coefficient of the sorption energy in the form (mmol^2 J^{-2}); ε is the Polanyi potential; R is the gas constant taken at a value of (8.314 J mol^{-1} K^{-1}); and T denotes the temperature in kelvins (K).

The fitting curve of the Dubinin–Radushkevich model is shown in Fig. 6. The values of constants β and E are presented in Table 2. The E-value calculated for the adsorption of S-DIB on MB is 25.01 kJ mol^{-1}, further suggesting that the adsorption mechanism can be described as chemical adsorption.

Adsorption kinetics. The adsorption kinetics mechanism of MB by S-DIB was investigated, including the proposed primary

Table 2 Fitting parameters of the Dubinin–Radushkevich model

β (mmol^2 J^{-2})	E (kJ mol^{-1})	R^2
7.99×10^{-10}	25.01	0.9371

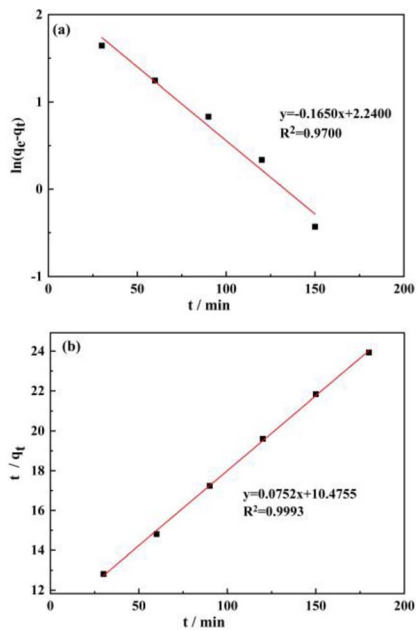

Fig. 7 (a) Pseudo-first-order model for the adsorption of MB on S-DIB and (b) pseudo-second-order model for the adsorption of MB on S-DIB.

Table 3 Fitting parameters for the pseudo-first-order and pseudo-second-order models for the adsorption of MB on S-DIB

Pseudo-first-order model			Pseudo-second-order model		
q_e (mg g^{-1})	K_1	R^2	q_e (mg g^{-1})	K_2	R^2
5.12	0.002	0.97	7.5	0.1146	0.9993

Table 4 Parameters of three periods in the intraparticle diffusion model for the adsorption of MB on S-DIB

Parameters	Period I	Period II	Period III
c	−5.373	6.1783	9.5763
k	2.0471	1.4368	0.0197
R^2	0.9994	0.9982	0.5543

model (Pfo) and the proposed secondary model (Pso), as given by eqn (7) and (8).[41,42] The linear fitting curves for the Pfo and Pso models are illustrated in Fig. 7(a) and (b), and the relevant parameters are listed in Table 3.

$$\ln(q_e - q_t) = \ln q_e - K_1 t \quad (7)$$

$$\frac{t}{q_t} = \frac{1}{K_2 q_e^2} + \frac{t}{q_e} \quad (8)$$

where t (min) is the adsorption reaction time, q_t (mg g^{-1}) is the adsorption capacity of MB after t minute, k_1 (g mg^{-1} min^{-1}) is the adsorption rate constant for the pseudo-first-order model, and k_2 (g mg^{-1} min^{-1}) is the adsorption rate constant for the pseudo-second-order model.

Compared with the R^2 of 0.9700 in the Pfo model, the Pso model with the R^2 value of 0.9993 was superior in accounting for the adsorption of MB onto S-DIB. In other words, the adsorption process of MB by S-DIB aligns more closely with the Pso model. Consequently, the kinetics of adsorption are predominantly governed by chemisorption mechanisms.

For an in-depth study of adsorption kinetics, the intraparticle diffusion model (Id) was employed to investigate this process, as presented in eqn (9):[43]

$$q_e = k_3 t^{1/2} + c \quad (9)$$

where c is a constant of the intraparticle diffusion model and k_3 is the rate constant for Id.

Initially (Fig. 8, stage I), the rate of intra-particle diffusion is fast, which is caused by the external mass transfer processes.[44] In the second stage (Fig. 8, stage II), MB diffuses slowly through the internal pores of S-DIB; the adsorption rate becomes relatively slow. In the last step (Fig. 8, stage III), the adsorption rate tends to be gentle in the final stage of adsorption. To better compare each linear stage of data fitting, the k and correlation coefficient R^2 of each stage are calculated separately,[45] and the results are shown in Table 4. The first part of the linear fitting of the experimental data using the intraparticle diffusion model was compared with the other two parts. The steeper slope is attributed to the dye MB molecules passing through the solution to the S-DIB surface; the second stage linear fitting describes the gradual adsorption of dye MB molecules by S-DIB. The last stage is due to the relatively low concentration of MB molecules in the solution. Internal diffusion begins to slow down, tends to balance, and finally reaches equilibrium. In the linear fitting curves, the straight line does not pass through the origin. The linear fitting degree of adsorption in the whole time range is not high, indicating that S-DIB has much force control in the process of adsorbing dyes and that internal diffusion is only one of the driving forces.

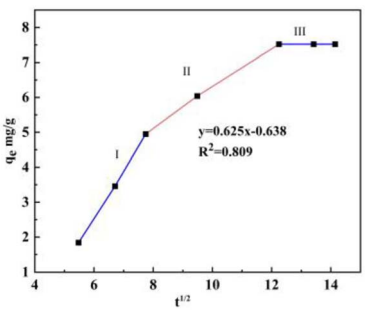

Fig. 8 Intraparticle diffusion model for the adsorption of MB on S-DIB.

Thermodynamic study. The thermodynamics of adsorption were explored to grasp the adsorption mechanism, and the influencing factors were investigated.

At ambient temperature, a series of adsorption experiments were carried out to determine the thermodynamic parameters: changes in enthalpy (ΔH), entropy (ΔS), and Gibbs free energy (ΔG). The Van't Hoff Equation was employed, as illustrated in eqn (10)–(12):[46]

$$nK_c = \frac{\Delta S}{R} - \frac{\Delta H}{RT} \quad (10)$$

$$\Delta G = -RT \ln K_c, \quad (11)$$

$$\Delta G = \Delta H - T\Delta S \quad (12)$$

where K_c is the adsorption equilibrium constant, R is the universal gas constant (8.314 J mol^{-1} K^{-1}), and T (K) is the absolute temperature. Fig. 9 shows a plot of $\ln K_c$ *versus* $1/T$ for MB adsorption by S-DIB. Basically, a linear relationship is observed, which indicates that the enthalpy change (ΔH) is temperature independent in the range of 293–318 K. The enthalpy change in MB on S-DIB was found to be in the range of $1/T$. Therefore, ΔH and ΔS values can be directly derived from the slope and intercept of the straight line, as demonstrated in Fig. 9, respectively. The thermodynamic parameters calculated for adsorbed MB are listed in Table 5. ΔG values are negative at all selected temperatures, which indicates that the adsorption process of MB is spontaneous. In addition, the negative ΔH values in Table 5 indicate that the adsorption reaction is exothermic. Meanwhile, the negative ΔS value indicates a decrease in the degree of freedom.

ΔG values are negative at all selected temperatures, indicating that the adsorption process of MB is spontaneous. In

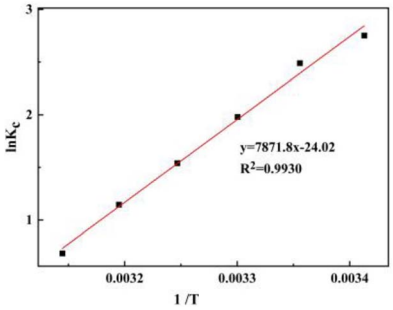

Fig. 9 Plot of ln K_c *vs.* 1/T for the MB adsorption by S-DIB.

Table 5 Thermodynamic parameters of MB adsorption by S-DIB

T (K)	K_c	ΔG (kJ mol^{-1})	ΔH (kJ mol^{-1})	ΔS (J mol^{-1} K^{-1})
293.15	15.67	−6.706	−31.42	−107.2
298.15	12.05	−6.170		
303.15	9.075	−5.559		
308.15	5.557	−4.394		
313.15	3.145	−2.983		
318.15	1.985	−1.813		

addition, the negative ΔH values in Table 5 indicate that the adsorption process is exothermic. Additionally, the negative ΔS value indicates a decrease in the degree of freedom.

Regeneration study. Sustainability and reusability are extremely significant factors for selecting adsorbents, and regeneration experiments are the principal methods for verifying these capabilities. The regeneration experiments were generated as follows: 20 mg S-DIB in 20 mL 8 mg L^{-1} MB solution was shaken for 180 min; then, the residue concentration of MB was measured by UV-vis. The S-DIB adsorbed with MB was eluted with an eluent (0.1 mol L^{-1} HCl aqueous : methanol = 1 : 1),[47] and the regenerated S-DIB was washed three times with distilled water for the next adsorption experiment. Fig. 10 illustrates the regeneration capabilities of S-DIB across three cycles.

Fig. 10 shows a decrease in MB adsorption efficiency from 96.53% to 65.46%. The results indicated that absorption efficiency gradually decreased with an increase in cycle times, which may be due to MB undergoing chemical adsorption processes and further entering the adsorbent.[48] Moreover, the elution efficiency of S-DIB during the regeneration experiments consistently exceeds 65%, indicating that it is an excellent regenerated copolymer and an efficient and environmentally friendly MB adsorbent.

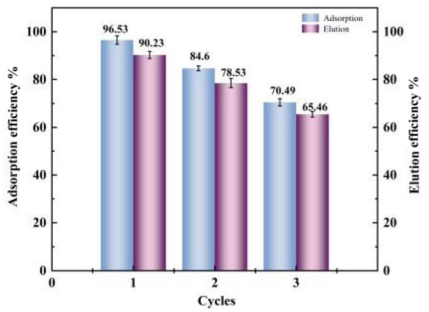

Fig. 10 Regeneration properties of S-DIB on MB adsorption.

Adsorption mechanism discussion. Based on the adsorption mechanism investigation above, the adsorption isotherms of S-DIB on MB fit better with the Langmuir model described as monolayer adsorption behavior; the adsorption kinetics are consistent with the Pso model as mainly chemical adsorption behavior, and the mean adsorption energy also suggests that the adsorption mechanism belongs to chemical adsorption.

Actually, the MB molecule includes a thiazine ring with sulfur and nitrogen atoms; the electron cloud around the sulfur atom produces an instantaneous uneven distribution of charge and forms an instantaneous dipole. The same occurs with the nitrogen atoms in the thiazine ring of MB and the sulfur atoms of S-DIB. As the two molecules of MB and S-DIB approach each other, these instantaneous dipoles interact reciprocally to produce dispersion forces and attract each other.[49]

Additionally, copolymer S-DIB has multiple benzene ring structures linked with C–C, C–S and S–S bonds, and the MB molecule consists of a phenothiazine ring and two aromatic rings forming a large conjugated aromatic ring with a more regular planar plane. Thus, both S-DIB and MB can provide delocalized π electron clouds. When the two molecules approach each other, they attract each other owing to the delocalization of π electrons, and π–π packing may occur. However, the planar properties of the S-DIB polymer are not ideal owing to the presence of branched chains and C–S bonds outside the benzene ring.[50]

In a word, during the adsorption process between the adsorbent and cationic dye molecule, the adsorption mechanism can be attributed to chemical adsorption, containing electrostatic attraction and π–π packing.

Photodegradation mechanism discussion. Sulfur atoms have larger dispersion and impurity energy levels in the conduction band, and the increase in the optical corresponding range indicates that more electrons can be generated, which can improve their photocatalytic performance.[51] In the photocatalytic degradation process, when the photon energy of visible light meets the S-DIB electron transition condition, it can be absorbed by S-DIB, and the electrons transition from the valence band to the conduction band, leaving holes in the valence band and forming photo generated electron hole pairs.[52]

According to the curve and calculations, the energy of the bandgap of 95% S-DIB can be achieved as 2.08 eV,[53] as shown in Fig. 11a. This reveals the favorable photodegradation characteristics of sulfur-rich polymers.[54–56] The photodegradation properties of polymers are modulated by varying the relative concentrations of monomers in the polymer backbone.[23]

The S-DIB materials with different sulfur mass ratios were investigated for their light absorbance using UV-vis spectra (Fig. 11b). The pure S_8 absorbed UV light from 200 nm to 500 nm, and the UV-vis spectra of 50%, 75% and 90% are

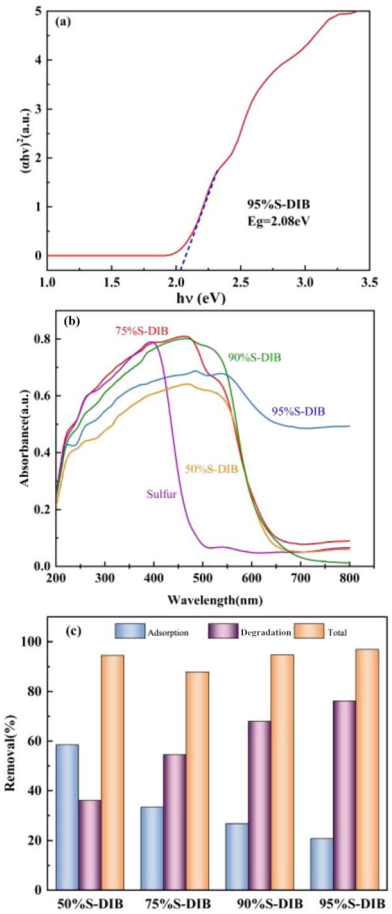

Fig. 11 (a) Tauc plot of 95% S-DIB. (b) Solid-state UV diffuse reflectance of S-DIB and sulfur with different sulfur contents. (c) Estimation of the contribution of the adsorption and photodegradation to the removal of MB using S-DIB with different sulfur contents.

similar in the absorption band shape, while 95% S-DIB has an absorption ranging from 200 nm to 650 nm.

Consequently, the photodegradation properties of S-DIB with varying sulfur content are systematically studied in Fig. 11c. Based on the experimental data, the adsorption performance declined as the sulfur content rose, while the photodegradation performance progressively improved. As an illustration, in the case of 50% S-DIB, the adsorption mechanism accounts for about 58.5% of the MB removal, while the photodegradation activity accounts for 36.1%. Conversely, 76.2% of the MB elimination in the case of 95% S-DIB is due to photodegradation, while 20.8% is due to the adsorption mechanism. Thus, 95% S-DIB has the best photodegradation capacity among the four S-DIB samples.

To further analyze the mechanism of photodegradation, the products generated from the degradation processes of MB by S-DIB were determined using UHPLC-MS.

As shown in Fig. 12, the UHPLC chromatograms of MB mixtures before and after 90 min and 180 min of photodegradation under irradiation have different retention times.[57,58] As time passes, the intensity and area of MB UHPLC peaks decrease. Moreover, the intermediate products related to

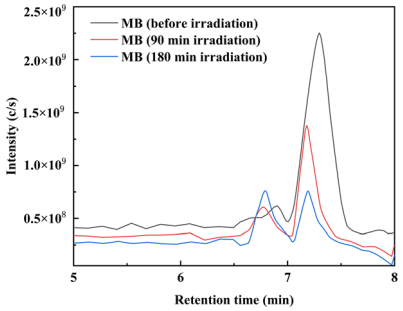

Fig. 12 UHPLC analysis of MB (initial solution of 8 mg L^{-1}).

the cationic dye MB during the photodegradation process can be detected through the demethylation cleavage of MB,[59] and the fragment ions of MB generated from photodegradation are shown in Fig. S9.†

Based on the reported literature,[60–63] the m/z signal of 284 can be attributed to the MB molecular ion (Fig. S10a†), while m/z 270 corresponds to the oxidation product of MB, which is Azure B (Fig. S10b†). During the photodegradation process, the ion at m/z 256 is a by-product of MB degradation, which is Azure A (Fig. S10c†). Therefore, the photodegradation mechanism of MB under irradiation can be described as follows. First, MB molecules undergo demethylation to yield Azure B with m/z 270, which is subsequently subjected to dealkylation, resulting in Azure A with signals of m/z 256.

These adsorption-photodegradation experimental results demonstrate that S-DIB can effectively break down the toxic cationic dye of MB with high concentrations under visible light.

Conclusions

In summary, there are electrostatic interactions, dispersion forces, and presumable π–π stacking interactions between S-DIB and MB, which promote the improvement of the adsorption efficiency and the regeneration performance. The experimental data fit the Pso kinetic model and Langmuir adsorption isotherm model well, confirming that the adsorption mechanism of MB can be attributed to chemical adsorption and monolayer adsorption on S-DIB. The mean adsorption energy obtained from the Dubinin Radushkevich model further confirmed the conclusion of chemical adsorption. Furthermore, the S-DIB copolymer effectively utilizes the energy of ultraviolet visible light to generate electron–hole pairs and generates its unique photodegradation properties.

S-DIB synthesized from a large amount of industrial by-product waste of sulfur can remove methylene blue from dye wastewater through a dual mechanism of adsorption and photodegradation. This study achieves the goal of waste treatment from waste and enriches the application of sulfur-rich polymers.

Data availability

The data supporting this article have been included as part of the ESI.†

Author contributions

MoYan Wu: Conceptualization, methodology, writing – original draft. Yue Liu: Experimental research, data processing. Lili Wu: Data processing. Tom Hasell: Writing – original draft, conceptual design. Fang Luan: Writing – original draft, supervision and project administration, funding acquisition.

Conflicts of interest

There are no conflicts to declare.

Acknowledgements

This work is supported by the China scholarship Council (CSC No. 202008230226).

References

1 M. Ismail, K. Akhtar, M. I. Khan, T. Kamal, M. A. Khan, M. A. A, J. Seo and S. B. Khan, *Curr. Pharm. Des.*, 2019, **25**, 3645–3663.
2 B. Kamenicka, P. Svec and T. Weidlich, *Int. J. Mol. Sci.*, 2023, **24**, 11235.
3 Y. Zhang, J. Liu, X. Du and W. Shao, *J. Eur. Ceram. Soc.*, 2019, **39**, 4891–4900.
4 S. S. Suryawanshi, P. P. Kamble, R. Gurav, Y.-H. Yang and J. P. Jadhav, *Biomass Convers. Biorefin.*, 2023, **13**, 5353–5366.
5 B. R. Mphuthi, P. M. Thabede, J. S. Modise, T. Xaba and N. D. Shooto, *Appl. Sci.*, 2023, **13**, 9659.
6 W. Zhang, H. Li, J. Tang, H. Lu and Y. Liu, *Molecules*, 2019, **24**, 469.
7 D. H. Nguyen, H. N. Tran, H.-P. Chao and C.-C. Lin, *Adsorpt. Sci. Technol.*, 2019, **37**, 607–622.
8 X. Ren, X. Shu, W. Geng, P. Li and Y. Xu, *Processes*, 2024, **12**, 773.
9 M. P. Crockett, A. M. Evans, M. J. Worthington, I. S. Albuquerque, A. D. Slattery, C. T. Gibson, J. A. Campbell, D. A. Lewis, G. J. Bernardes and J. M. Chalker, *Angew. Chem., Int. Ed.*, 2016, **55**, 1714–1718.
10 R. Priyadarshi, A. Khan, P. Ezati, S. K. Tammina, S. Priyadarshi, T. Bhattacharya, J. T. Kim and J.-W. Rhim, *Environ. Chem. Lett.*, 2023, **21**, 1673–1699.
11 T. Zhang, G. Xing, W. Chen and L. Chen, *Mater. Chem. Front.*, 2020, **4**, 332–353.
12 A. Nayeem, M. F. Ali and J. H. Shariffuddin, *Environ. Res.*, 2023, **216**, 114306.
13 J. J. G. Woo Jin Chung, E. T. Kim, H. Yoon, A. G. Simmonds, H. J. Ji, P. T. Dirlam, R. S. Glass, J. J. Wie, N. Nguyen, B. W. Guralnick, J. Park, A. Somogyi, P. Theato, M. E. Mackay, Y. E. Sung, K. Char and J. Pyun, *Nat. Chem.*, 2013, **5**, 518–524.
14 X. Li, L. Yuan, D. Liu, Z. Li, J. Chen, K. Yuan, J. Xiang and Y. Huang, *Energy Storage Mater.*, 2020, **26**, 570–576.
15 S. Shukla, A. Ghosh, U. K. Sen, P. K. Roy, S. Mitra and B. Lochab, *ChemistrySelect*, 2016, **1**, 594–600.
16 R. Zou, W. Liu and F. Ran, *InfoMat*, 2022, **4**, e12319.
17 T. Thiounn, M. K. Lauer, M. S. Bedford, R. C. Smith and A. G. Tennyson, *RSC Adv.*, 2018, **8**, 39074–39082.
18 P. Yan, W. Zhao, S. J. Tonkin, J. M. Chalker, T. L. Schiller and T. Hasell, *Chem. Mater.*, 2022, **34**, 1167–1178.
19 M. Lee, S. G. Jang, H. Yeo, J. J. Park, B. Moon and N.-H. You, *Macromolecules*, 2024, **57**, 2905–2914.
20 Z. Ren, X. Jiang, L. Liu, C. Yin, S. Wang and X. Yang, *J. Mol. Liq.*, 2021, **328**, 115437.
21 M. J. H. Worthington, R. L. Kucera, I. S. Albuquerque, C. T. Gibson, A. Sibley, A. D. Slattery, J. A. Campbell, S. F. K. Alboaiji, K. A. Muller, J. Young, N. Adamson, J. R. Gascooke, D. Jampaiah, Y. M. Sabri, S. K. Bhargava, S. J. Ippolito, D. A. Lewis, J. S. Quinton, A. V. Ellis, A. Johs, G. J. L. Bernardes and J. M. Chalker, *Chem–Eur. J.*, 2017, **23**, 16219–16230.
22 R. L. Upton, R. A. Dop, E. Sadler, A. M. Lunt, D. R. Neill, T. Hasell and C. R. Crick, *J. Mater. Chem. B*, 2022, **10**, 4153–4162.
23 M. J. H. Worthington, R. L. Kucera and J. M. Chalker, *Green Chem.*, 2017, **19**, 2748–2761.
24 A. S. Farioli, M. V. Martinez, C. Barbero, E. Yslas and D. Acevedo, *J. Appl. Polym. Sci.*, 2023, **141**, e54914.
25 A. Leon-Vaz, J. Cubero-Cardoso, A. Trujillo-Reyes, F. G. Fermoso, R. Leon, C. Funk, J. Vigara and J. Urbano, *Chemosphere*, 2023, **315**, 137761.
26 H. Berk, M. Kaya, M. Topcuoglu, N. Turkten, Y. Karatas and A. Cihaner, *React. Funct. Polym.*, 2023, **187**, 105581.
27 V. Diniz, J. C. Bear, S. Rath and C. R. Crick, *Sci. Rep.*, 2024, **14**, 8144.
28 E. Santoso, R. Ediati, Y. Kusumawati, H. Bahruji, D. O. Sulistiono and D. Prasetyoko, *Mater. Today Chem.*, 2020, **16**, 100233.
29 I. Anastopoulos, M. J. Ahmed, V. E. Ojukwu, M. Danish, M. Stylianou and J. O. Ighalo, *J. Mol. Liq.*, 2023, **394**, 123719.
30 V. K. S. Wadi, K. K. Jena, S. Z. Khawaja, K. Yannakopoulou, M. Fardis, G. Mitrikas, M. Karagianni, G. Papavassiliou and S. M. Alhassan, *ACS Omega*, 2018, **3**, 3330–3339.
31 K. Choi, W. Jang, W. Lee, J. S. Choi, M. Kang, J. Kim, K. Char, J. Lim and S. G. Im, *Macromolecules*, 2022, **16**, 7222–7231.
32 J. Castañeda-Díaz, T. Pavón-Silva, E. Gutiérrez-Segura and A. Colín-Cruz, *J. Chem.*, 2017, **1**, 1–14.
33 J. Zhu, S. C. Qi, X. Q. Liu and L. B. Sun, *Chem. Commun.*, 2023, **56**, 8700–8703.
34 W. Wei, L. Jiao, W. Li, X. Tang, W. Xie, H. Yu, W. Li and F. Lei, *Food Control*, 2023, **145**, 109410.
35 S. Soni, P. K. Bajpai, J. Mittal and C. Arora, *J. Mol. Liq.*, 2020, **314**, 113642.
36 P. Saini, N. Chakinala, P. K. Surolia and A. G. Chakinala, *Sep. Purif. Technol.*, 2024, **354**, 128730.
37 W. Ruan, H. Liu, H. Wu, Y. Qi, M. Zhou, C. Zhou, Z. Zhang and H. Yang, *Fuel Process. Technol.*, 2022, **236**, 10743.
38 B. Gaur, J. Mittal, S. A. A. Shah, A. Mittal and R. T Baker, *Molecules*, 2024, **10**, 2387.
39 R. Agarwala and L. Mulky, *ChemBioEng Rev.*, 2023, **3**, 326–335.
40 J. T. Phiri and S. Oh, *Sustainability*, 2024, **16**, 6342.

41 S. Jin, A. Sen and A. W. Sandvik, *Phys. Rev. Lett.*, 2012, **108**, 045702.
42 F. C. Wu, R. L. Tseng, S. C. Huang and R.-S. Juang, *Chem. Eng. J.*, 2009, **151**, 1–9.
43 G. F. Malash and M. I. El-Khaiary, *Chem. Eng. J.*, 2010, **163**, 256–263.
44 S. Chatterjee, T. Chatterjee and S. H. Woo, *Chem. Eng. J.*, 2011, **166**, 168–175.
45 F. Wei, S. Jin, C. Yao, T. Wang, S. Zhu, Y. Ma, H. Qiao, L. Shan, R. Wang, X. Lian, X. Tong, Y. Li, Q. Zhao and W. Song, *Molecules*, 2023, **28**, 4426.
46 Y. Q. Yan, X. D. Sun, H. X. Wang, Y. M Fu and Z. L. Xiu, *Sep. Purif. Technol.*, 2018, **199**, 351–358.
47 F. Li, J. Liu, W. Liu, Y. Xu, Y. Cao, B. Chen and M. Xu, *RSC Adv.*, 2021, **41**, 25551–25560.
48 R. K. O. Alivio, A. W. Go, A. E. Angkawijaya, S. P. Santoso, C. Gunarto and F. E. Soetaredjo, *J. Environ. Chem. Eng.*, 2015, **3**, 2172–2179.
49 S. Wang, Y. Xin, H. Hu, X. Su, J. Wu, Q. Yan, J. Qian, S. Xiao and Y. Gao, *RSC Adv.*, 2022, **12**, 35445–35451.
50 A. Abbasi, I. Ahmad, H. H. Abd El-Gawad, W. A. Alshahrani, N. D. Alqarni, Z. M. El-Bahy and S. Ikram, *Int. J. Biol. Macromol.*, 2024, **259**, 129221.
51 J. Chakraborty, I. Nath and F. Verpoort, *Chem. Soc. Rev.*, 2022, **51**, 1124–1138.
52 R. L. Upton, R. A. Dop, E. Sadler, A. M. Lunt, D. R. Neill, T. Hasell and C. R. Crick, *J. Mater. Chem. B*, 2022, **10**, 4153–4162.
53 N. R. K. O. Alivio, A. W. Go, A. E. Angkawijaya, S. P. Santoso, C. Gunarto, F. E. Soetaredjo, Q. Tufts, N. C. Chiu, E. N. Musa, T. C. Gallagher, D. B. Fast and K. C. Stylianou, *Chem–Eur. J.*, 2023, **29**, e202203177.
54 S. Ghosh, H. Küçükkeçeci, R. P. Paitandi, V. Weigelt, V. Dippold, S. Seki and A. Thomas, *J. Mater. Chem. A*, 2023, **1**, 247–255.
55 N. Corrigan, S. Shanmugam, J. Xu and C. Boyer, *Chem. Soc. Rev.*, 2016, **45**, 6165–6212.
56 H. Wang, S. Jin, X. Zhang and Y. Xie, *Angew. Chem., Int. Ed. Engl.*, 2020, **59**, 22828–22839.
57 J. Chakraborty, I. Nath and F. Verpoort, *Chem. Soc. Rev.*, 2022, **51**, 1124–1138.
58 M. I. Al-Zaban, M. A. Mahmoud and M. A. AlHarbi, *Saudi. J. Biol. Sci.*, 2021, **28**, 2007–2013.
59 D. T. Nguyen, H. N. Nguyen, T. M. Nguyen, H. C. Dong, N. N. Dang, Q.-H. Tran, T. A. Nguyen, M. Van Tran, T. Le Hoang Doan, L. C. Luu and M. Van Nguyen, *Colloids Surf., A*, 2024, **689**, 133663.
60 N. Martin and Y. Leprince-Wang, *Phys. Status Solidi A*, 2021, **218**, 2100532.
61 G. J. Van Berkel, A. D. Sanchez and J. M. E. Quirke, *Anal. Chem.*, 2002, **74**, 6216–6223.
62 V. K. Gupta, M. Sharma and R. K. Vyas, *J. Environ. Chem. Eng.*, 2015, **3**, 2172–2179.
63 S. Hisaindee, M. A. Meetani and M. A. Rauf, *TrAC, Trends Anal. Chem.*, 2013, **49**, 31–44.